Numerical modelling of hybrid arc/laser welding: a coupled approach to weld bead formation and residual stresses

Olivier Desmaison, Gildas Guillemot, Michel Bellet

▶ **To cite this version:**

Olivier Desmaison, Gildas Guillemot, Michel Bellet. Numerical modelling of hybrid arc/laser welding: a coupled approach to weld bead formation and residual stresses. JOM17, International Conference on Joining Materials, May 2013, Helsingor, Denmark. 11 p. hal-00983421

HAL Id: hal-00983421

https://hal-mines-paristech.archives-ouvertes.fr/hal-00983421

Submitted on 25 Apr 2014

HAL is a multi-disciplinary open access archive for the deposit and dissemination of scientific research documents, whether they are published or not. The documents may come from teaching and research institutions in France or abroad, or from public or private research centers.

L'archive ouverte pluridisciplinaire **HAL**, est destinée au dépôt et à la diffusion de documents scientifiques de niveau recherche, publiés ou non, émanant des établissements d'enseignement et de recherche français ou étrangers, des laboratoires publics ou privés.

Proc. JOM17, Int. Conf. on Joining Materials, May 5-8, 2013, Helsingor, Denmark, International Institute of Welding (2013) 11 pages

Numerical modelling of hybrid arc/laser welding: a Level Set approach for weld bead formation and residual stresses

Olivier DESMAISON*, Gildas GUILLEMOT*, Michel BELLET*
** Mines ParisTech - Centre de Mise en Forme des Matériaux (CEMEF), CNRS UMR 7635,*
Rue Claude Daunesse, BP 207, 06904 Sophia-Antipolis, France
Olivier.Desmaison@mines-paristech.fr, Gildas.Guillemot@mines-paristech.fr, Michel.Bellet@mines-paristech.fr

ABSTRACT

The joining of high thickness steel sheets by means of hybrid Laser/GMAW welding processes is studied in this paper. A three dimensional finite element model has been developed to simulate this process. Through an ALE framework, a level set approach is used to model the interface between the metal and the surrounding gas. Even though the physics of the plasma is not modelled, both thermal and material supply phenomena are taken into account: (i) The laser and GMAW heat sources are simulated and applied on the interface through the Continuum Surface Force method, (ii) An original method of volume element expansion has been chosen to simulate the material supply and the bead formation. A thermo mechanical problem resolution has been settled in this model. Depending on the thermal evolution of the mechanical parameters and on the velocity field, the material behaviour will be elastic, elasto-visco-plastic or visco-plastic. The ALE approach enables to compute the stresses inside the workpiece and to obtain the displacements of the workpiece borders. Two finite elements models are presented to illustrate: (i) A hybrid arc/laser welding simulation through the thermal and material supply resolution, (ii) A TIG welding simulation through the stress and strain mechanical resolution.

1. INTRODUCTION

The range of welding process's use in joining operations has recently expanded thanks to the emergence of hybrid arc / laser processes. Indeed, the coupling of a laser beam with a gas metal arc torch enhances the efficiency of gas metal arc welding (GMAW) processes. Located ahead of the torch, this new heat source provides additional energy to the workpiece. The resulting weld pool spreading enables to supply more material, to mix it more homogeneously and consequently to weld better and faster.

Nevertheless, the complexity of coupled thermo-mechanical phenomena induced by this new process increases. Therefore, a deeper understanding is required regarding the heat transfer from the heat sources and the molten droplets to the weld pool and the heat affected zone. Actually, the neighbourhood of the fusion zone is where deformations and stresses form first. These stresses may lead to hot tearing for some critical alloys and highlights the need for an accurate numerical modelling.

Recent models have shown their ability to realistically simulate GMAW processes taking into account the main thermal and fluid flow phenomena inside both the arc plasma and the weld pool [1, 2, 3]. Such heat and fluid flow approaches have been recently applied to hybrid arc/laser melting, especially with the objective of simulating the effect of laser, through direct or indirect modelling of keyhole phenomena [4, 5, 6, 7, 8]. As a result, the calculated shapes of weld beads better fit the experimental ones.

Research in hybrid welding process simulations has not been yet extended to stress/strain computation. The analysis of stress/strain formation during and after welding is generally achieved through uncoupled thermal-mechanical calculations to, further, study hot cracking phenomena induced by the process [10, 11] or residual stresses in the final workpiece [12, 13, 14]. In fact, while the thermal field strongly impacts the residual stress field, the stress field affects with a low influence the thermal field.

The present paper reports on a transient three dimensional finite element model that has been developed to simulate the weld bead forming during hybrid laser/GMAW process. The model considers both a consumable electrode and a laser beam moving along a workpiece. However, the electrode, the arc plasma, the droplets and the laser beam are not explicitly represented. The model includes the workpiece and a surrounding gaseous domain for which different boundary conditions are expressed. During the formation of the weld bead, firstly, the energy equation is solved. The material supply is taken into account thanks to the level set approach, the interface between the surrounding gas/air and the workpiece being defined by a signed distance function. The

resolution of Navier-Stokes equations, including first a mass source term to account for material supply, and second surface tension forces, gives access to the velocity field, which is used to transport and update the level set interface. The uncoupled resolution of the thermal-mechanical problem begins then. From the temperature distribution, the mechanical properties of the 316L steel are derived. According to the material state, elasto-visco-plastic, visco-plastic or Newtonian, the stresses and strains in the heat affected zone and in the base metal are computed.

The paper presents first the mathematical formulation for the heat & material supply. A simulation of a hybrid arc/laser welding process is carried out to analyse the model efficiency. A comparison between the weld bead cut planes from simulation and experimentation is proposed. Next, the mechanical solver is detailed. A simulation of a TIG welding process is presented. To the best of our knowledge, it is the first time that Level Set approach and stress & strain computation are coupled. To validate the presented model a comparison between both approaches with and without LS is carried out.

2. MATHEMATICAL FORMULATION FOR A GMAW SIMULATION

2.1. Level Set approach

A Eulerian approach is used in which the interface between the metal and the surrounding air or plasma is defined by a level set function. This choice is justified by the modelling of multi-pass hybrid arc/laser welding processes [16] and the objective to model arc plasma in a future extended version of the model. A nodal signed distance function φ is defined to represent the interface between gas and metal. Because the governing mass, energy and momentum equations are solved in the entire finite element domain, as illustrated in FIGURE 1, a smooth interface transition of the thermal properties is needed. Near the interface a mixed property law is defined using a sinusoidal Heaviside function $H(\varphi)$:

$$H(\varphi)=1/2\left[1+\varphi/\varepsilon+1/\pi\left(\sin\pi\varphi/\varepsilon\right)\right] \text{ for } \varphi\in\left[-\varepsilon,+\varepsilon\right] \quad (1)$$

The mixed law is restricted to a $[-\varepsilon,+\varepsilon]$ domain perpendicular to the surface defined by $\varphi(t)=0$. Denoting α_{gas} and α_{metal} the values of a physical variable in both domains, the averaged or mixed value α is defined by:

$$\alpha=\alpha_{metal}[1-H(\varphi)]+H(\varphi)\alpha_{gas} \quad (2)$$

All model's physical parameters such as the density ρ, the specific heat C_p, the thermal conductivity λ or the viscosity η, are computed according to this mixing rule, using the same Heaviside function.

2.2. Heat transfer: energy equation

The transient energy equation solved to obtain the temperature T in the whole domain is the following:

$$\rho C_p\left(\frac{\partial T}{\partial t}+\vec{v}\cdot\vec{\nabla}T\right)-\vec{\nabla}\cdot\left(\lambda\vec{\nabla}T\right)=\dot{Q} \quad (3)$$

where ρ, C_p and λ are the thermal properties computed from Eq. (2). All of them are temperature dependant and their value varies with the liquid fraction. $\vec{v}$ is the velocity vector. In this model the temperature homogeneisation resulting from the fluid flow in the weld pool is only taken into account through an enhanced liquid thermal conductivity. Nevertheless the velocity field $\vec{v}$ is not equal to zero (see §2.4). The study of flows in the weld pool from the model described in this paper is detailed in [17].

Two heat sources have to be considered in a hybrid laser/arc welding simulation. The first one consists in the heat supplied by the arc plasma for which a surface Gaussian distribution of the heat input is supposed. The model relies on thermal radiation physics: the input heat flux q_P through the surface depends on the opening angle of the arc plasma, the distance to the electrode and the orientation of the surface normal vector with respect to the direction of the torch. The second heat source is associated with the laser beam. In the present model, a defocused laser beam of moderate power is supposed for which no keyhole phenomenon is observed.

The heat input is then modelled through a surface heat flux q_L with a Gaussian distribution and an area limited to the laser radius. Both sources - plasma and laser - are expressed through surface boundary conditions. In the present context of level set formulation, the *Continuum Surface Force* developed by Brackbill *et al.* [18] has to be used to transform them into volumetric heat input conditions, appearing as right hand side terms $\dot{Q}$ in Eq. (3). Therefore the Dirac function $\delta(\varphi)$ – that is the derivative of the Heaviside function $H(\varphi)$ (Eq. (1), the integral of which over $[-\varepsilon,+\varepsilon]$ is 1) – is used to define the two volumetric heat sources: $\dot{Q}_P = q_P \delta(\varphi)$ and $\dot{Q}_L = q_L \delta(\varphi)$.

The heat provided to the fusion zone by the impingement of molten droplets represents the last heat source $\dot{Q}_D$. Based on the volumetric model of Lancaster [19] and improved later by Kumar and Bhaduri [20], it consists in defining a cylinder below the arc/plasma in the weld pool into where an additional source term is imposed. The appropriate dimensions of the cylinder are discussed in [21]. Finally three heat source terms are added to the right hand side of the energy equation (3):

$$\dot{Q} = (q_P + q_L)\delta(\varphi) + \dot{Q}_D \tag{4}$$

Convective heat transfer and emissivity are taken into account too. They are imposed as a *Fourier* condition along the borders of the finite element model. On the interface, they are computed as:

$$\dot{Q}_T = \left(h(T - T_{ext}) + \varepsilon\sigma(T^4 - T_{ext}^4)\right)\delta(\varphi) \tag{5}$$

where h is the heat transfer coefficient, ε the emissivity, σ the Boltzmann constant and T_{ext} the ambient temperature. The heat losses $\dot{Q}_T$ are subtracted to the final heat source term of Eq. (4). FIGURE 1 represents the different heat sources applied on the model.

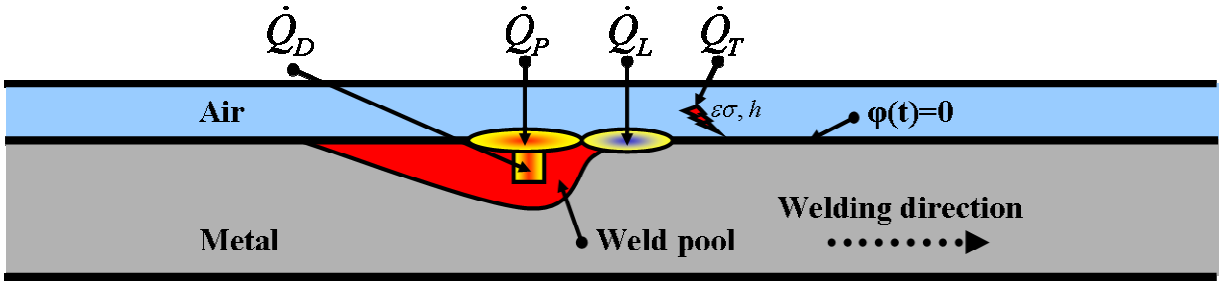

FIGURE 1: Schematics of the heat sources considered in the finite element model, in level set formulation.

2.3. Material supply: mass & momentum equation

An original method has been settled to model material supply [21]. A volume expansion source term $\dot{\theta}$ is added to the right hand side of the mass conservation equation for finite elements contained in the cylindrical zone introduced in the previous paragraph. $\dot{\theta}$ is computed as a function of the geometrical dimensions of the electrode and the welding parameters. The coupled mass and momentum equations are the compressible Navier-Stokes ones:

$$\begin{cases} \rho\left(\dfrac{\partial \vec{v}_{\dot{\theta}}}{\partial t} + \vec{v}_{\dot{\theta}} \cdot \vec{\nabla}\vec{v}_{\dot{\theta}}\right) - \vec{\nabla} \cdot \overline{\overline{s_{\dot{\theta}}}} + \vec{\nabla} p_{\dot{\theta}} = \vec{F} \\ \vec{\nabla} \cdot \vec{v}_{\dot{\theta}} = \dot{\theta} \end{cases} \tag{6}$$

The computed velocity field $\vec{v}_{\dot{\theta}}$ will be used then to transport the interface as explained next. A Newtonian behaviour is considered for the metal such as:

$$\overline{\overline{s_{\dot{\theta}}}} = 2\eta \overline{\overline{e_{\dot{\theta}}}} \quad \text{with} \quad \overline{\overline{e_{\dot{\theta}}}} = \frac{1}{2}\left(\vec{\nabla}\vec{v}_{\dot{\theta}} + {}^t\vec{\nabla}\vec{v}_{\dot{\theta}}\right) - tr\left(\frac{1}{2}\left(\vec{\nabla}\vec{v}_{\dot{\theta}} + {}^t\vec{\nabla}\vec{v}_{\dot{\theta}}\right)\right)\overline{\overline{I}} \tag{7}$$

where η is the viscosity and $\overline{\overline{\dot{e}_{\dot{\theta}}}}$ the strain rate tensor computed from the velocity $\vec{v}_{\dot{\theta}}$. As previously, the viscosity is computed from Eq. (2) and it is temperature dependant. An enhanced value of the liquid viscosity is used for a stronger stabilization of the mechanical resolution. The right hand side term of the momentum equation, $\vec{F}$, includes two forces which apply onto the free surface. The first one is the gravity, $\vec{F}_g$. The second one is the surface tension. First a surface force vector is defined as a function of the distance function:

$$\vec{T}_\gamma = \kappa\,\gamma\,\vec{n} \tag{8}$$

where the mean curvature κ and the normal vector $\vec{n}$ are computed as:

$$\vec{n} = \vec{\nabla}\varphi \Big/ \left\|\vec{\nabla}\varphi\right\| \quad \text{and} \quad \kappa = -\nabla\cdot\vec{n} \tag{9}$$

As this force is a surface force, once again, the *Continuum Surface Force* has to be applied. The final term $\vec{F}$ is equal to:

$$\vec{F} = \vec{F}_g + \vec{T}_\gamma\delta(\varphi) \tag{10}$$

The arc pressure is neglected in this model.

2.4. Weld bead shaping: transport & reinitialization of the Level Set

Once the velocity field associated with material supply is computed, the interface has to be transported. In this way, the following convection equation is solved:

$$\frac{\partial\varphi}{\partial t} + \vec{v}_{\dot{\theta}}\cdot\vec{\nabla}\varphi = 0 \tag{11}$$

The new Level Set φ=0 is the updated interface. A reinitialization step is then realized to respect the Eikonal property on the field φ: $\left\|\vec{\nabla}\varphi\right\| = 1$. The modelling of the material supply step (§2.3 &§2.4) is illustrated in FIGURE 2. Moreover, because of the Eulerian approach used in this resolution, the temperature field must to be transported too. Therefore, the velocity field $\vec{v}$ of the energy equation (3) is equal to $\vec{v}_{\dot{\theta}}$.

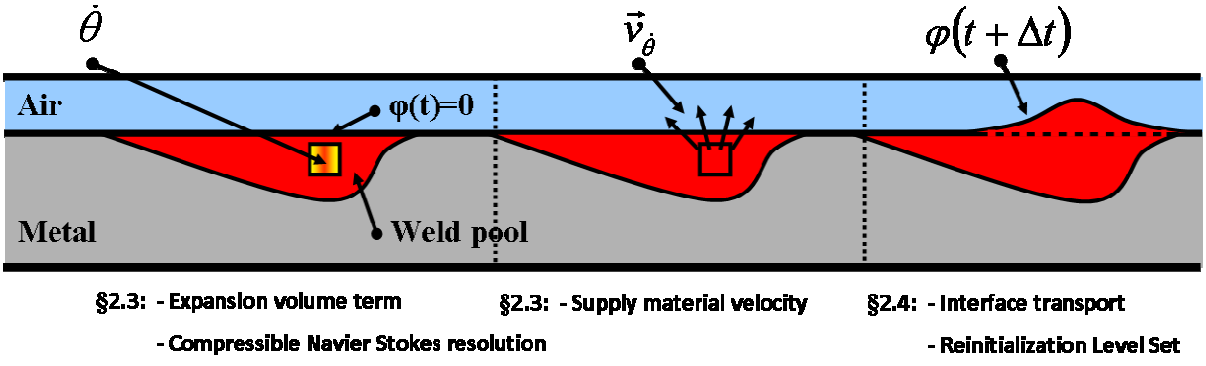

FIGURE 2: Illustration of the different steps of the supply material modelling.

3. HYBRID LASER/GMAW PROCESS SIMULATION

3.1. Model description

The simulation of a hybrid laser/GMAW welding is proposed to illustrate the previous mathematical simulation. The simulated process consists in the filling of a narrow chamfer (FIGURE 3). The metal is the low alloyed 18MND5 steel. Its properties, thermal dependant, are taken from the commercial software *ThermoCalc*. The interface between the machinated chamfer and the gas is defined by the level set function. A hybrid heat source moves along the workpiece to form the weld bead. It is composed of a GMAW electrode and a 3 mm radius laser beam located 3 mm ahead. The power of the laser beam is 6000 W and the torch power is around 10000 W, assumed to be divided in two parts: 70% for the arc plasma source and 30% for melting the electrode metal into droplets [21]. The velocity of the torch is 13.3 mm/s, the velocity and the diameter of the wire are respectively v_w = 200 mm/s and Φ_w = 1.2 mm. A value of 20 [15] is used for the enhanced conductivity factor to model the weld pool mixture. Only one pass is simulated and the results are presented in the next section.

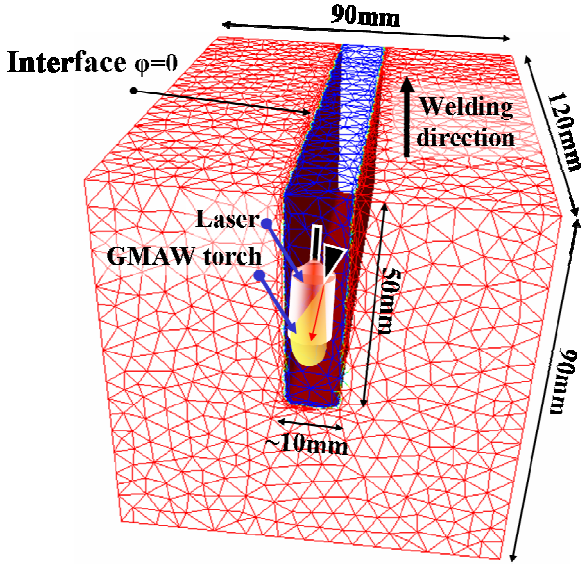

FIGURE 3: FE model for the simulation of a hybrid Laser/GMAW process simulation.

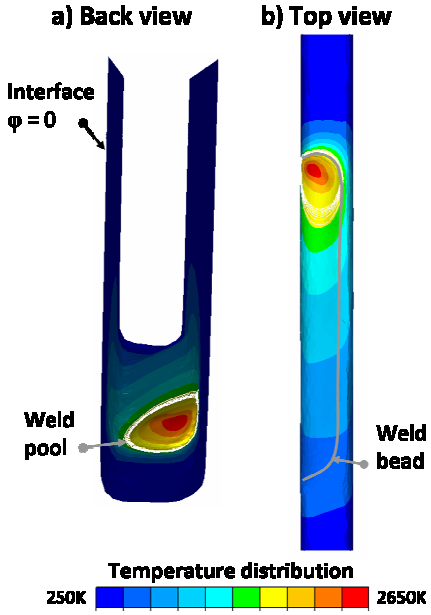

FIGURE 4: Two views of the numerical weld bead. Temperature distribution at the interface.

3.2. Results

The modelled weld bead is presented on the FIGURE 4. Its final shape is visible on the back view (a) and the interface temperature distribution on the top view (b).

Two comparisons are proposed to validate this model. First, on the FIGURE 5, the obtained size of the weld pool free surface is compared to the one measured from a picture. This latter comes from a fast acquisition camera movie. The simulated weld bead pool is 18mm long and 9.6mm large. Its dimensions are very close to the experimented ones: 20.1mm long and 10mm large. A second comparison from experimentation and simulation has been carried on the FIGURE 6 for a transversal weld bead cut. The numerical weld bead is less convex than the real one. This is due to an enhanced viscosity of the liquid metal. Its volume is 7% larger than the one supplied. The droplet density / weld pool density ratio is not taken into account in the computation of the expansion term $\dot{\theta}$ and overestimates the material supply. Its impact on the mass conservation does not seem to be negligible and it could explain the difference of 7%. On contrary the experimental measured volume is 4% lower than the volume supplied. It may be due to the vaporization of the liquid metal and the droplets projected out of the weld pool. Moreover, the borders of the weld pool are very different. In the experiment case the pool is more depth and narrower. This “finger” shape is induced by the droplets fall. In the presented

model, the flows inside the weld pool are not taken into account. So, the mixture of the material does not occur which explains the curved shape of the weld pool.

Nevertheless the similarity between the simulation and the experimentation keeps very good. It proves the efficiency of the present model. A fluid flows model could be improve the results.

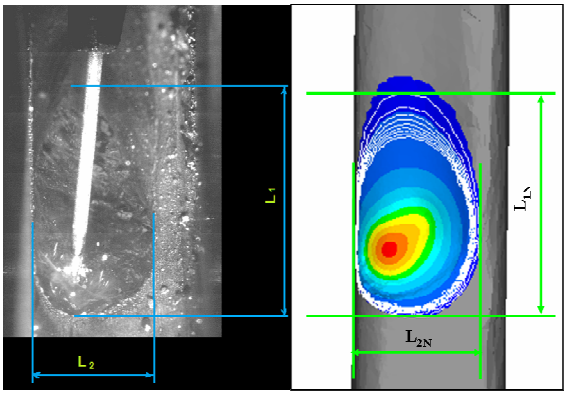

a) Experimentation b) Simulation

FIGURE 5: Comparison of the weld pool size between experimentation (a) and simulation (b).

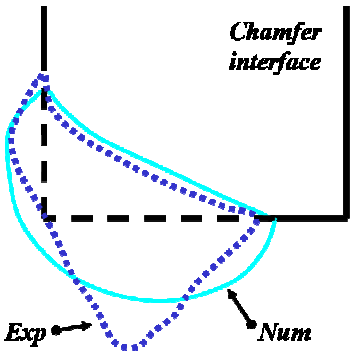

FIGURE 6: Superimposition of the weld bead from the experimentation (Exp) and the numerical simulation (Num).

4. RESIDUAL STRESSES: BEHAVIOUR LAW & MECHANICAL EQUATION

Like all models found in the literature, this model is uncoupled. The thermal distribution field and the weld bead shaping computations are separated from the mechanical resolution. Indeed the residual stress computation is carried out from the final model state after energy, mass and momentum equations resolution at each time step.

The mechanical problem to be solved is the following:

$$\begin{cases} \rho\left(\frac{\partial \vec{v}_S}{\partial t} + \vec{v}_S \cdot \vec{\nabla}\vec{v}_S\right) - \vec{\nabla} \cdot \overline{\overline{s_S}} + \vec{\nabla} p_S = \vec{F} \\ \nabla \cdot \vec{v}_S = tr\left(\underline{\underline{\dot{\varepsilon}^{el}}}\right) + tr\left(\underline{\underline{\dot{\varepsilon}^{th}}}\right) \end{cases} \quad (12)$$

The solutions are the velocity of the material $\vec{v}_S$ and the pressure *p*. The right hand side term of the equation, $\vec{F}$, corresponds to the body forces. Here, only the gravity force is considered. The term $\dot{\varepsilon}^{el}$ represents the elastic part of the strain rate tensor and the term $\dot{\varepsilon}^{th}$ the thermal one. The deviatoric stress tensor $\overline{\overline{s_S}}$ in Eq. (12) directly derives from the velocity field $\vec{v}_S$ through the material behaviour law. As this is done at the centre of tetrahedral elements, no mixing law is required here. Indeed, according to the state of the element (gas or metal) and its centre temperature, the kind of resolution will not be the same. Three different behaviours are defined in this model:

- The gas or surrounding air is considered as an incompressible fluid. Its behaviour is Newtonian (N). The deviatoric stress tensor $\overline{\overline{s_S}}$ is defined as:

$$\overline{\overline{s_S}} = 2\eta_{gas}\bar{\bar{e}} \quad (13)$$

where η_{gas} is the dynamic viscosity of the gas. Its value is very low and, as expected, stresses in the gas part of the model are negligible. The strain rate tensor $\bar{\bar{e}}$ is computed as in Eq. (7) from the velocity $\vec{v}_S$.

- If the metal has a temperature lower than a critical temperature T_C (usually chosen as the solidus temperature) its behaviour is elastic-visco-plastic (EVP). A multiplicative behaviour law is used in the present model. The equivalent stress is computed as:

$$\bar{\sigma} = K_{EVP}\dot{\bar{\varepsilon}}^{m_{EVP}}\bar{\varepsilon}^{n} + \sigma_Y \tag{14}$$

where K_{EVP}, m_{EVP} and n are respectively the EVP consistency, the EVP strain-rate sensitivity and the hardening coefficient. σ_y is the yield stress. These four material parameters are temperature dependant. The equivalent strain $\bar{\varepsilon}$ is an input from the previous time step whereas the equivalent strain rate $\dot{\bar{\varepsilon}}$ depends on the velocity $\vec{v}_S$.

- If the metal has a temperature higher than the critical temperature T_C, its behaviour is visco-plastic (VP). The Norton-Hoff law is applied to express the deviatoric stress tensor:

$$\overline{\overline{s_S}} = 2K_{VP}\left(3\dot{\bar{\varepsilon}}_P\right)^{0.5(m_{VP}-1)}\overline{\overline{\dot{e}}} \tag{15}$$

where K_{VP}, m_{VP} are respectively the VP consistency and the VP strain-rate sensitivity which are temperature dependant.

Moreover, the temperature influence on the residual stress computation is also taken into account through the mass conservation equation of Eq. (12). Indeed, the thermal part of the strain rate tensor $\dot{\varepsilon}^{th}$ depends on the thermal evolution of the density:

$$tr\left(\overline{\overline{\dot{\varepsilon}^{th}}}\right) = 3\alpha\dot{T} = 3\left(-\frac{1}{3\rho(T)}\frac{\partial\rho(T)}{\partial T}\right)\frac{\partial T}{\partial t} = -\frac{1}{\rho(T)}\frac{\partial\rho(T)}{\partial t} \tag{16}$$

This mechanical problem is non linear due to the velocity dependence of the behaviour law. So a Newton-Raphson method has to be used. After convergence, the iterative resolution provides the nodal velocity and pressure fields $\vec{v}_S$ and p. From the velocity field $\vec{v}_S$ and the mechanical time step Δt_M the nodal displacements are computed:

$$x^{t+\Delta t} = x^{t} + \vec{v}_S\,\Delta t_M \tag{17}$$

Whereas in the material supply resolution a Eulerian approach is used (the velocity field $\vec{v}_\theta$ is used to transport the interface and the temperature), in this part, a Lagrangian approach is considered. In fact, the mesh is convected by the velocity field $\vec{v}_S$. So the impact of the mechanical resolution on the level set function and the interface is also taken into account.

5. RESIDUAL STRESSES COMPUTATION IN TIG WELDING

5.1. Model description

The 3D finite elements model consists in a thick plate of austenitic steel 316L. The dimensions are given on the FIGURE 7. Two domains coexist: the gas in the top part and the metal below. Around the interface plane, φ = 0, the mesh is refined for a correct definition of the mixing law (Eq. (1)) and to be able to efficiently use the *Continuum Surface Force* method (Eq. (4)).

The torch is moving along the *x*-axis on the centre of the plate with a velocity of 1mm/s. The plate sides, which are parallel to the welding direction, are fixed: their displacement is null, $\vec{v}_S = 0$. This welding configuration has been proposed by Hamide, [15]. In order to illustrate the presented mechanical resolution of this model, a comparison of numerical results with a LS approach and without is proposed here. Indeed, to the best of our knowledge it is the first time that a stress and strain computation is carried out from a welding simulation including a level set approach. The thermal and mechanical material properties of the 316L are given in [15]. The TIG heat source is circular with a power P_P of 975W and a radius r_P of 5mm:

$$\dot{Q}_P = \frac{P_P}{\pi\, r_p^2} \tag{18}$$

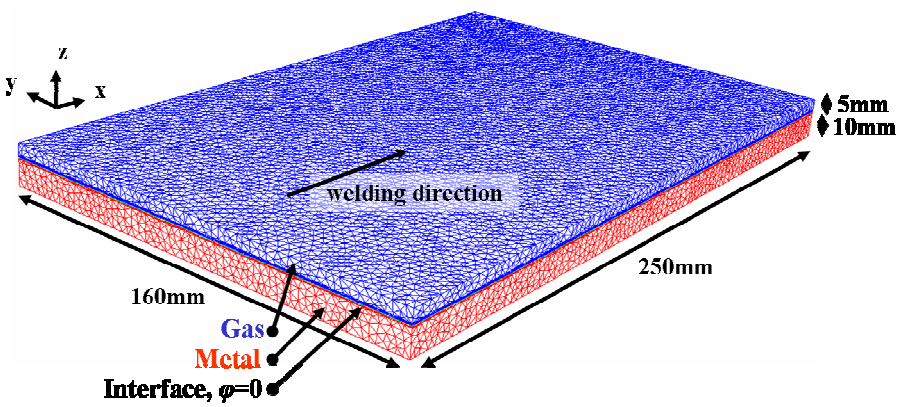

FIGURE 7: Model description.

5.2. Numerical validation of the mechanical computation

A sensor is located at a distance of 95mm ahead the plate front side, at a depth of φ = -5mm and on the weld bead axis. The numerical longitudinal (*x* direction) and transversal (*y* direction) stresses from both models with and without Level Set are compared on the FIGURE 8. The curves tendency is respected. Only the maximum values of tensile and compressive stresses are bigger with the Level Set approach. This is due to the meshes which are different. In fact, as the mechanical computation is realized at the element centre, according to position of the sensor in the element, the result could be a bit different. The thermal resolution is solved at each integration point of the element. So, the mesh has a lowest impact on the thermal measurement: both curves are identical. The computation of stresses from the present model with a level set approach is so considered validate. This result is significant because it is the first time that mechanical computation, level set approach and welding simulation are gathered in a same FE model.

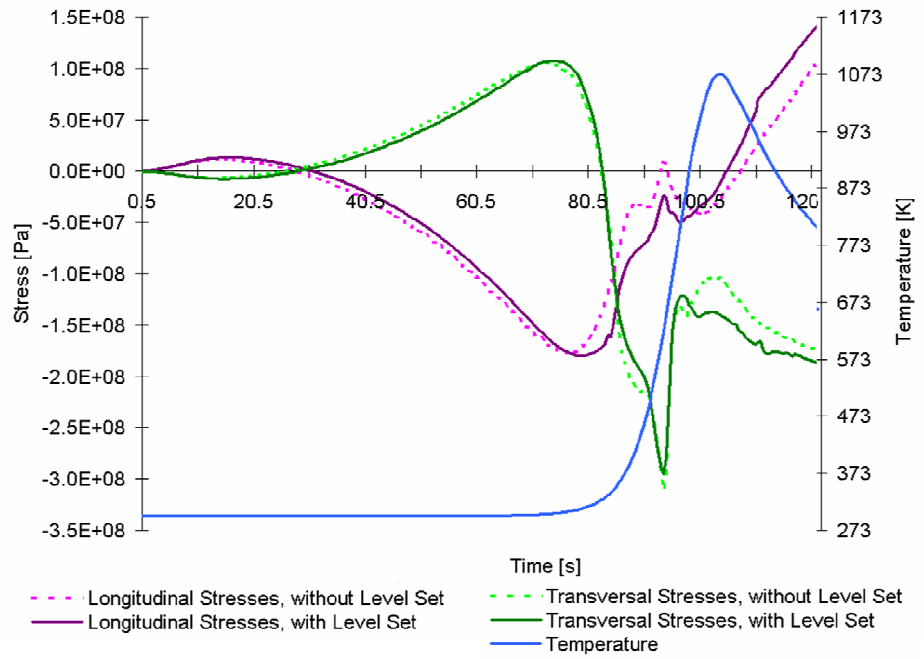

FIGURE 8: Comparison of the numerical stresses from both with and without Level Set models.

The residual stresses distribution on the plate top face after a welding of 95s is presented on the FIGURE 9. The lines represent the isothermal distribution. The maximal temperature is around 1660K which corresponds to a liquid fraction of 55%. The main stresses are located in the isothermal line 720K, the second one.

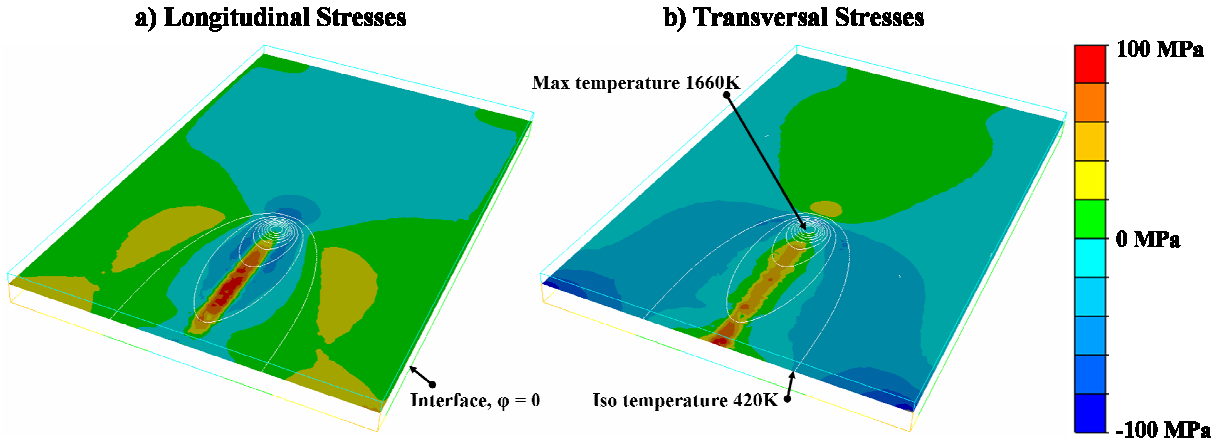

FIGURE 9: Longitudinal (a) and transversal (b) stress distribution on the interface.

To highlight the different behaviour of the steel plate, a last graph is proposed (FIGURE 10). The behaviour is visco-plastic where the temperature is upper than the solidus temperature, 1598K. A thick band at each part of the weld pool has an elasto-visco-plastic behaviour where the compressive stresses are the highest. Everywhere else the behaviour is elastic.

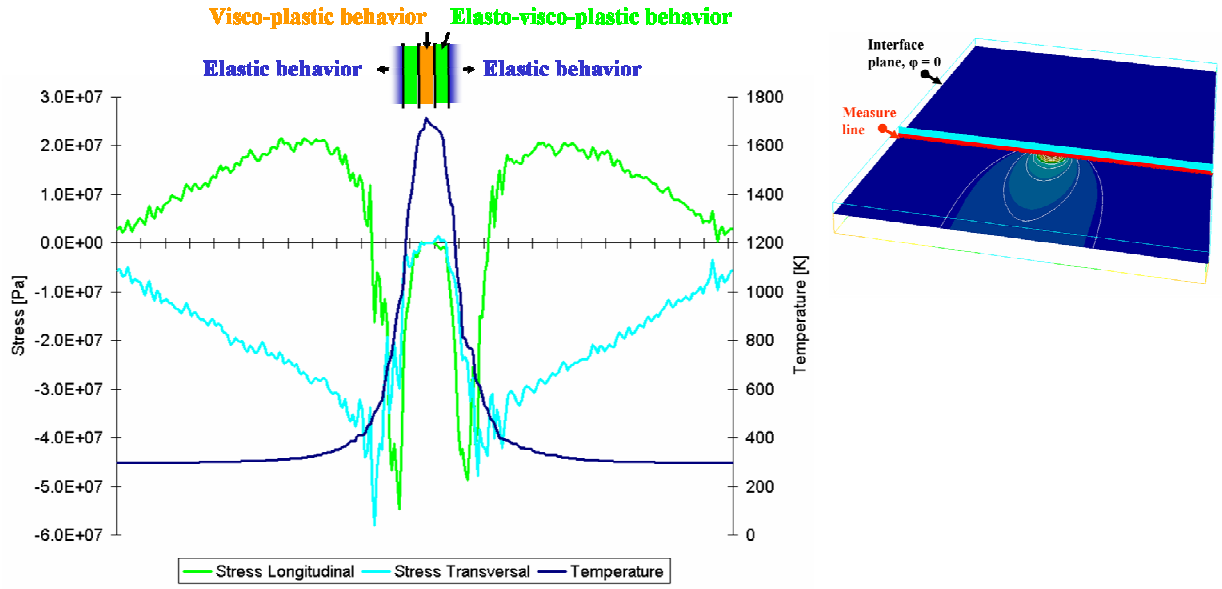

FIGURE 10: Evolution of the interface stresses according to the torch distance.

6. CONCLUSION

In this paper, a 3D finite element model has been described. Its main faculties are to allow the simulation of hybrid arc/laser welding, from the heat and mass supply to the residual stresses computation. Two cases have been proposed to illustrate both the parts of the paper.

An industrial hybrid welding process simulation has been carried out to highlight the model efficiency to model the weld bead growth. Weld pool dimensions and shape have been compared to the experiment. The Level Set approach used in this model will next allow realizing multi-pass welding simulation. Only one pass has been shown in this paper, but several ones could be presented during the speaking.

The mechanical computation is also possible with this model. Indeed, from a non coupled resolution and the thermal distribution as input, the model is able to compute the stresses induced by the welding heat source

supply. No industrial case has been proposed to validate this aspect of the model. A comparison between the model with a Level Set approach and without has sooner be shown. In fact, it quite unusual to compute mechanical stresses from a Level Set approach and it seem important to show that the model meets the criteria. A case with material supply could be presented during the speaking.

REFERENCES

[1] J. Hu and H.L. Tsai. Heat and mass transfer in gas metal arc welding. part i: The arc. *International Journal of Heat and Mass Transfer*, 50:833–846, 2007.

[2] J. Hu and H.L. Tsai. Heat and mass transfer in gas metal arc welding. part ii: The metal. *International Journal of Heat and Mass Transfer*, 50:808–820, 2007.

[3] G. Xu, J. Hu, and H.L. Tsai. Three-dimensional modelling of arc plasma and metal transfer in gas metal arc welding. *International Journal of Heat and Mass Transfer*, 52:1709–1724, 2009.

[4] H. Ki, J. Mazumder, and P. Mohanty. Modelling of laser keyhole welding: Part i. mathematical modelling, numerical methodology, role of recoil pressure, multiple reflections, and free surface evolution. *Metallurgical and Materials Transactions A*, 33:1817–1830, 2002.

[5] H. Ki, J. Mazumder, and P. Mohanty. Modelling of laser keyhole welding: Part ii. simulation of keyhole evolution, velocity, temperature profile, and experimental verification. *Metallurgical and Materials Transactions A*, 33:1831–1842, 2002.

[6] H. Zhao and T. Debroy. Macroporosity free aluminum alloy weldments through numerical simulation of keyhole mode laser welding. *Journal of Applied Physics*, 93:10089–10097, 2003.

[7] R. Rai, S.M. Kelly, R. P. Martukanitz, and T. DebRoy. A convective heat-transfer model for partial and full penetration keyhole mode laser welding of a structural steel. *Metallurgical and Materials Transactions*, 39:98–112, 2008.

[8] T. Zhang, C.S. Wu, G.L. Qin, X.Y. Wang, and S.Y. Lin. Thermomechanical analysis for laser + gmaw-p hybrid welding process. *Computational Materials Science*, 47:848–856, 2010.

[9] A. Traidia and F. Roger. Numerical and experimental study of arc and weld pool behaviour for pulsed current gta welding. *International Journal of Heat and Mass Transfer*, 54:2163–2179, 2011.

[10] Y. Danis, E. Lacoste, and C. Arvieu. Numerical modeling of inconel 738lc deposition welding: Prediction of residual stress induced cracking. *Journal of Materials Processing Technology*, 210:2053–2061, 2010.

[11] Y.H. Wei, Z.B. Dong, R.P. Liu, and Z.J. Dong. Three-dimensional numerical simulation of weld solidification cracking. *Modelling and Simulation in Materials Science and Engineering*, 13:437–454, 2005.

[12] R.V. Preston, H.R. Shercliff, P.J. Withers, and S. Smith. Physically-based constitutive modelling of residual stress development in welding of aluminium alloy 2024. *Acta Materialia*, 52:4973–4983, 2004.

[13] B. Taljat, B. Radhakrishnan, and T. Zacharia. Numerical analysis of gta welding process with emphasis on post-solidification phase transformation effects on residual stresses. *Material Science and Engineering A*, 246:45–54, 1998.

[14] F. Kong and R. Kovacevic. Modeling of heat transfer and fluid flow in the laser multilayered cladding process. *Metallurgical and Materials Transactions B*, 41:1310–1320, 2010.

[15] M. Hamide. *Modélisation numérique du soudage à l'arc des aciers*. PhD thesis, Mines ParisTech, 2008.

[16] O. Desmaison, G. Guillemot, and M. Bellet. Modelling of the bead formation during multi pass hybrid laser/gas metal arc welding. In *proceedings of LASERAP'7, Séminaire européen sur les applications des lasers de puissance*, île d'Oléron, France, 1-5 octobre 2012.

[17] O. Desmaison, G. Guillemot, and M. Bellet. A multi-physics level set approach for the simulation of the hybrid laser / gmaw process. In *proceedings of IWS conference, 10th Int. Seminar on Numerical Analysis of Weldability*, Seggau, Austria, 24 - 26 September 2012.
[18] J.U. Brackbill, D.B. Kothe, and C. Zemach. A continuum method for modelling surface tension. *Journal of Computational Physics*, 100:335–354, 1991.
[19] J.F. Lancaster. The physics of welding. *Physics in technology*, 15, 1984.
[20] S. Kumar and S.C. Bhaduri. Three-dimensional finite element modelling of gas metal-arc welding. *Metallurgical Transactions B*, 25:435–441, 1994.
[21] M. Bellet and M. Hamide. Direct modelling of material deposit and identification of energy transfer in gas metal arc welding. *International Journal of Numerical Methods for Heat & Fluid Flow*, Accepted, 2012.